MIXED–PHASE STRATIFORM CLOUD SYSTEM MODEL AND CASE MODELING ON TWO LOW–LEVEL MESOSCALE VORTICES

Liu Gongbo (刘公波), *Hu Zhijin* (胡志晋) and *You Laiguang* (游来光)

Institute of Weather Modification, Chinese Academy of Meteorological Sciences, Beijing 100081

Received August 29, 1992

ABSTRACT

We introduced the two–parameter stratiform cloud model of Hu and Yan (1986) into the mesoscale model of Anthes et al. (1987), and reprogramed the latter, then constructed a three–dimensional stratiform cloud system model which includes three phases of water and detailed cloud physical processes. For the stability and accuracy of calculation in a larger time step, we accepted a set of hybrid–schemes for all and the time split scheme for some of the cloud physical processes, and proposed a parameterized method which calculates different types of phase change processes simultaneously, and designed the falling schemes of particles following the Lagrangian method.

We used a dry model, a cumulus parameterization model, a two–phase explicit scheme model, and the model presented here to simulate two low–level mesoscale vortices, compared and analysed the simulating capability of these models. The results show that in simulation of the circulation structure of meso–vortex, the structure of cloud system, and surface precipitation, the model presented here is more reasonable and closer to the observations than other models.

Key words: stratiform cloud system, case modeling, low–level mesoscale vortex, 3D cloud model

1. INTRODUCTION

The stratiform cloud system model is an important tool to study physical processes of precipitation in cloud system and the possibility of artificial precipitation. There have been some mixed–phase microphysical models of stratiform clouds (Buekov and Pernach, 1975; Rutledge and Hobbs, 1983; Hu and Yan, 1986; Liu et al., 1988), in which the microphysical processes and artificial precipitation in different dynamic backgrounds were studied and simulated in detail. But these models were limited to one or two dimensions and their dynamic fields of environment were given, so it is difficult for them to be used in wider range problems. In the last decade, more and more attention was paid to the cloud physical processes in hydrostatic mesoscale models and a two–phase explicit scheme was added in PSV / NCAR's MM4 model (Anthes et al., 1987). With a three–dimensional mixed–phase model, Zhang (1989) simulated the influence of ice–phase cloud physical processes on mesoscale atmospheric motion. Furthermore, Pernach (1988) and Heimann (1990) simulated the ideal front with mixed–phase mesoscale models respectively, but they did not simulate a real case, and not analyse the microstructures of cloud and precipitation mechanism. It is very meaningful to simulate the physical process of cloud and precipitation in the real atmosphere. In the current mesoscale models, the MM2 model (Anthes and Warner, 1978) has been tested by Institute of Mesoscale Meteorology of CAMS and has showen a certain accuracy and computational stability. It is more important that it can

be initialized with observational data. As the physical processes in this model are simple and the structure of program is very complicated, we reprogramed and partially modified the model according to MM4, then introduced and partially modified a detailed two-parameter microphysical model (Hu and Yan, 1986), and finally constructed a three-dimensional mesoscale model which could be used to simulate the real case of mixed-phase cloud system. In order to test the model, we selected the mesovortex, one of important precipitation systems in China, as the object of simulation. In this paper we mainly test the simulating capability of the model. Precipitation mechanism of cloud systems and interaction between cloud physical processes and dynamic processes etc. will be discussed in another paper.

II. MODEL DESCRIPTION

1. *Dynamic Equations and Differential Scheme*

The dynamic equations and differential schemes are taken from Anthes et al. (1987). In the geopotential equation the load of ice phase hydrometeors is added:

$$\frac{\partial\varphi}{\partial\ln(\sigma+P_t/P^*)} = -RT_v\left(1+\frac{q_c+q_r+q_i+q_s}{1+q_v}\right)^{-1} \tag{1}$$

and the diabatic heating by phase change is added to prognostic equation of temperature (see formula (4) in this paper). The vertical coordinate is the P–σ coordinate, here $\sigma=(P-P_t)/P^*$, $P^*=P_s-P_t$, and P_s, P_t are the surface and model top pressure respectively. The grid has the spatial staggered structure; variables P^*u, P^*v are staggered with the others in horizontal, and $\dot{\sigma}$ is staggered with the others in vertical direction. The numbers of grid points for three dimensions (x, y, σ) are $31\times31\times10$. The differential scheme is the leapfrog integration scheme, and the temporal integration scheme comes from Brown and Campana (1978).

2. *The Cloud Microphysical Equations and Parameterized Scheme*

Eight microphysical variables are considered: the specific mass of vapor, cloud, rain, ice and snow (q_v, q_c, q_r, q_i, q_s), and the concentrations of particles of rain, ice and snow (N_r, N_i, N_s). Eleven microphysical processes are considered: ice nucleation (*PVI*), the deposition and evaporation of ice (*SVI*) and of snow (*SVS*), the condensation and evaporation of cloud (*CON*) and the evaporation of rain (*SVR*), the autoconversions of ice to snow (*AIS*) and cloud to rain (*ACR*), the melting of ice crystals into cloud droplets (*MIC*) and of snow flakes into cloud droplets (*MSC*) and rain drops (*MSR*), the collections of cloud droplets by snow and rain particles (*CCS*, *CCR*). Before the symbols denoting these processes, we add a "*W*" to express the changing rate of mass and an "*N*" to express the changing rate of concentration.

Cloud physical equations:

$$\frac{\partial P^*q_\alpha}{\partial t} = -\left(\frac{\partial P^*uq_\alpha}{\partial x}+\frac{\partial P^*vq_\alpha}{\partial y}\right)-\frac{\partial P^*\dot{\sigma}q_\alpha}{\partial\sigma}+P^*\frac{\delta q_\alpha}{\delta t}+Fq_\alpha, \tag{2}$$

$$\frac{\partial P^*N_\alpha}{\partial t} = -\left(\frac{\partial P^*uN_\alpha}{\partial x}+\frac{\partial P^*vN_\alpha}{\partial y}\right)-\frac{\partial P^*\dot{\sigma}N_\alpha}{\partial\sigma}+P^*\frac{\delta N_\alpha}{\delta t}+FN_\alpha, \tag{3}$$

where specific mass content $q_\alpha=\rho_\alpha/\rho_d$. The unit for all variables in this model is in MKS system. The diabatic heating concerning phase change is

$$Q = (WCON + WSVR)L_v + (WSVI + WSVS)L_s + (WMIC + WMSC + WMSR + WCCS)L_f. \tag{4}$$

Sources and sinks:

$$\frac{\delta q_c}{\delta t} = WCON + WMIC + WMSC - WACR - WCCS - WCCR, \tag{5}$$

$$\frac{\delta q_r}{\delta t} = WACR + WCCR + WMSR - WSVR - WVR, \tag{6}$$

$$\frac{\delta q_i}{\delta t} = WPVI + WSVI - WAIS - WMIC - WVI, \tag{7}$$

$$\frac{\delta q_s}{\delta t} = WAIS + WCCS + WSVS - WMSC - WMSR - WVS, \tag{8}$$

$$\frac{\delta q_v}{\delta t} = -(WCON - WSVR + WSVI + WSVS), \tag{9}$$

$$\frac{\delta N_i}{\delta t} = NPVI - NSVI - NAIS - NMIC - NVI, \tag{10}$$

$$\frac{\delta N_s}{\delta t} = NACS - NSVS - NMSC - NMSR - NVS, \tag{11}$$

$$\frac{\delta N_r}{\delta t} = NACR - NSVR + NMSR - NVR, \tag{12}$$

where VR, VI and VS represent changes of raindrops, ice crystals and snow flakes in falling.

The spatial differential scheme: for advection we used improved upstream scheme (Soony and Ogura, 1973), and for the descent of particles we used the method described in Section V of this paper. A hybrid scheme is used for temporal integration: leapfrog scheme for advection, semi-implicit scheme for sources and sinks (e.g. compute $\partial q_\alpha / \partial t$, $\partial N_\alpha / \partial t$ and q_α^{t+1}, N_α^{t+1} by using estimated values of q_α^*, N_α^*, T^* and $(P^*)^*$ that are obtained before calculating sources and sinks), and a small time step is used in calculating ACR, CCR and VR.

3. *Cloud Physical Processes*

The basic cloud physical model used here is written by Hu and Yan (1986). The distribution of the parameters is rewritten in metric system as follows:

distribution of cloud droplets:

$$\lambda_c = \left(\frac{10\pi\rho_w N_{0c}}{\rho_d q_c}\right)^{1/3}, \qquad \frac{N_c}{\rho_d} = \text{const.},$$

distribution of rain drops:

$$\lambda_r = \left(\frac{\pi\rho_w N_r}{\rho_d q_r}\right)^{1/3}, \qquad N_{0r} = \lambda_r N_r, \qquad \overline{V}_r = \frac{a\Gamma(4+b)}{6\lambda_r^b},$$

$$a = 842 \ \mathrm{m}^{0.2}/\mathrm{s}, \qquad b = 0.8,$$

distribution of ice and snow particles:

$$\lambda_\alpha = \left(\frac{6A_{m\alpha}N_\alpha}{\rho_d q_\alpha}\right)^{1/2}, \qquad N_{0\alpha} = \lambda_\alpha^2 N_\alpha, \qquad \overline{V}_\alpha = \frac{\Gamma(4\frac{1}{3})A_{v\alpha}}{\Gamma(4)\lambda_\alpha^{1/3}},$$

$$A_{mi} = 0.01\ \mathrm{kg/m^3}, \qquad A_{ms} = 0.03\ \mathrm{kg/m^3},$$

$$A_{vi} = 3.28\ \mathrm{m^{2/3}/s}, \qquad A_{vs} = 6.96\ \mathrm{m^{2/3}/s},$$

in these formulas $N_{0\alpha}$ and λ_α are spectrum parameters ($\mathrm{m^{-4}}$, $\mathrm{m^{-1}}$), $\overline{V}_\alpha$ is the mass-weighted average falling speed of particle group (m / s).

Saturation specific humidity with respect to water

$$q_{sw} = 6.11\exp\left(19.84659 - \frac{5418.12}{T}\right). \tag{13}$$

Saturation specific humidity with respect to ice

$$q_{si} = 6.11\exp\left(22.51 - \frac{6148.8316}{T}\right). \tag{14}$$

Ice nucleation

$$WPVI = NPVI \cdot q_{i0},\ NPVI = -BIN \cdot (CIN \cdot N_{i0})\frac{\mathrm{d}T}{\mathrm{d}t},\quad \text{if } T < 0℃ \text{ and } \frac{\mathrm{d}T}{\mathrm{d}t} < 0.$$

The initial mass of an ice crystal $q_{i0} = 10^{-9}$ g, $BIN = 0.342$, N is the concentration of activated ice nuclei. $CIN = \min\{1, 3.688\mathrm{e}^{-0.0003Z}\}$ is the fitting coefficient of ice nucleus number distribution with height according to You et al. (1982).

A scale conversion method is used for autoconversion of ice to snow (Hu and He, 1987). Define $D^* = 340\ \mu$m as the dividing point of ice and snow:

$$WAIS = \left(1 + \beta + \frac{\beta^2}{2} + \frac{\beta^3}{6}\right)e^{-\beta} q_i,$$

$$NAIS = (1+\beta)e^{-\beta} N_i, \qquad \beta = \lambda_i D^*.$$

Kessler method is used for ACR:

$$WACR = \begin{cases} K_1(q_c - q_{c0}), & q_c > q_{c0} \\ 0, & q_c < q_{c0} \end{cases} = 0.5\ \mathrm{g/kg},\ K_1 = 10^{-3}\ \mathrm{s^{-1}}.$$

The initial parameter $\lambda_{r0} = 385.726\ (\rho_d \cdot WACR)^{-0.247}$ is given according to M–P distribution and observational results (Mason, 1971), so the initial number of raindrops

$$NCAR = \frac{\rho_d \cdot WACR \cdot \lambda_{r0}^3}{\pi \rho_w}.$$

Collection of cloud droplets by snow

$$WCCS = \frac{\pi}{4}\Gamma\left(4\tfrac{1}{3}\right)A_{vs} q_c \overline{E}_{sc} \lambda_s^{-7/3} N_s e^{-\beta_1}\left(1 + \sum_{i=1}^{5}\beta_1^i / i!\right),$$

here $\beta_1 = \lambda_c D_c^*$, $D_c^* = 15\ \mu$m is the smallest scale of cloud droplets which can be collected by snow, $\overline{E}_{sc}$ is average collection efficiency.

Collection of cloud droplets by raindrop

$$WCCR = \frac{a\pi N_r \Gamma(3+b) q_c}{4\lambda^{2+b}}.$$

For ice and snow in the region $T > 0℃$, melting processes are completed in one time step, except that the melt mass exceeds the amount defined by thermal equilibrium equation:

$$WMIC = \frac{\delta_1 q_i^*}{\Delta t}, \quad WMIS = \delta_1 q_s^* / \Delta t \quad , \text{ if } T^* > 0℃, \quad \max\{q_i^*, q_s^*\} \neq 0$$

$$WMIC = 0, \qquad WMIS = 0, \qquad \text{others}$$

$$\delta_1 = \begin{cases} mildmax / m, & \text{if } m > mildmax \\ 1, & \text{if } m \leqslant mildmax \end{cases}$$

where $mildmax = (T^* - 273.16)C_p / L_f$, $m = q_i^* + q_s^*$. Ice particles melt into cloud droplets, but snow particles melt into cloud droplets and rain drops according to the minimum raindrop size $D^* = 200\ \mu m$:

$$WMSR = \int_D^\infty \cdot \frac{\pi}{6}\rho_w D^3 N_{r0} e^{-\lambda_s' D} dD = WMIS\left(1 + \beta + \frac{\beta^2}{2} + \frac{\beta^3}{6}\right)e^{-\beta},$$

$$WMSC = WMIS - WMSR, \qquad WMSC = NMIS - NMSR,$$

$$NMIC = \frac{WMIC \cdot N_i}{q_i}, \qquad NMIS = \frac{WMIS \cdot N_s}{q_s},$$

$$NMSR = \int_D^\infty \cdot N_{r0} e^{-\lambda_s' D} dD = NMIS(1+\beta)e^{-\beta},$$

where $\beta = \lambda_s' D^*$, $\lambda_s' = [\pi\rho_w(NMSR + NMSC)/(WMIS \cdot \rho_d)]^{1/3}$ is the distribution parameter of melted snow.

4. *Deposition, Condensation and Evaporation*

The key to computational stability of phase change is to control the variation of saturation level. Assign α^* as the estimated values of prognostic and diagnostic variables at $t+1$, Δt as time step, $\Delta S_w^* = q_v^* - q_{sw}^*$, $\Delta S_i^* = q_v^* - q_{si}^*$, $\Delta S_{wi}^* = q_{sw}^* - q_{si}^*$, so the maximum condensation and deposition are $\Delta q_c = r_1 \Delta S_w^*$ and $\Delta q_i = r_2 \Delta S_i^*$ according to the thermal equilibrium method, the condensation coefficient and deposition coefficient could be written as

$$r_1 = \left(1 + \frac{L_v}{C_p} 5418.12 \frac{q_{sw}^*}{T^{*2}}\right)^{-1}, \qquad r_2 = \left(1 + \frac{L_s}{C_p} 6148.8316 \frac{q_{si}^*}{T^{*2}}\right)^{-1}.$$

This method has been used in some models (Anthes et al., 1987; Zhang, 1989), but it exaggerates the deposition and evaporation; therefore it is necessary to consider a scheme that includes rates of phase changing.

The deposition, condensation and evaporation under three types of phase distributions are considered:

a. without ice phase ($T^* > 0℃$, or $\max\{q_i^*, q_s^*\} = 0$ and $\Delta S_i^* < 0$);

b. without liquid phase ($\max\{q_c^*, q_r^*\} = 0$ and $\Delta S_w^* < 0$);

c. with mixed-phase ($T^* < 0℃$ and $\max\{q_i^*, q_s^*\} \neq 0$ and $\max\{q_c^*, q_r^*\} \neq 0$, or $T^* < 0℃$

and $\Delta S_w^* > 0$, or $T^* < 0$℃ and $\max\{q_c^*, q_r^*\} \neq 0$ and $\Delta S_i^* > 0$).

The evaporation and condensation rates of rain drops are negligible, compared with that of cloud droplets, so that the condensation is omitted, and the evaporation is computed only when the air is under saturation after all of the cloud water evaporates or there are not any cloud droplets. The evaporation rate of rain drops:

$$SVR = \frac{2\pi \Delta S_w^* N_r^* [0.78\lambda_r^{-1} + 0.32 S_c^{1/3} (a/\gamma)^{1/2} \Gamma(2.9) \lambda_r^{-1.9}]}{q_{sw}^* \rho_d [(K_D \rho_d q_{sw}^*)^{-1} + (R_v T^{*2} D_T)^{-1}]},$$

$$WSVR = -\max\{SVR,\ r_1 \Delta S'_w / \Delta t,\ -q_r^* / \Delta t\},$$

$$r_1 \Delta S'_w = \begin{cases} r_1 \Delta S_w^*, & \text{if } q_c^* = 0,\ q_r^* > 0,\ \Delta S_w^* < 0 \\ r_1 \Delta S_w^* - WCON \cdot \Delta t, & \text{if } -r_1 \Delta S_w^* > q_c^* > 0,\ q_r^* > 0,\ \Delta S_w^* < 0 \\ 0. & \text{others} \end{cases}$$

a) For the first type of phase distribution described above,

$$WCON = \max\{r_1 \Delta S_w^* / \Delta t,\ -q_c^* / \Delta t\}.$$

b) For the second one, the growth rate of deposition:

$$\frac{dm_\alpha}{dt} = 2a_1 \left(\frac{N_\alpha^*}{\rho_d}\right)^{1-a_2} \left(\frac{q_\alpha^*}{6}\right)^{a_2} 10^{-3(1-a_2)},$$

here a_1 and a_2 are functions of temperature.

Equivalent deposition coefficients are denoted as

$$r_{i2} = \left(\frac{dm_i}{dt} / \Delta S_i^*\right)\Delta t, \qquad r_{s2} = \left(\frac{dm_s}{dt} / \Delta S_i^*\right)\Delta t,$$

so

$$WSVI = \max\{r_{i2} \delta_2 \Delta S_i^* / \Delta t,\ -q_i^* / \Delta t\},$$

$$WSVS = \max\{r_{s2} \delta_2 \Delta S_i^* / \Delta t,\ -q_s^* / \Delta t\},$$

here

$$\delta_2 = \begin{cases} 1, & \text{if } r_2 \geqslant r_{i2} + r_{s2} \\ r_2 / (r_{i2} + r_{s2}). & \text{if } r_2 < r_{i2} + r_{s2} \end{cases}$$

δ_2 ensures that the phase change process ends at most at the ice-saturation point.

c) For the third type of phase distribution, three schemes are proposed under three different saturation states:

c1) Supersaturation with respect to water ($\Delta S_w^* > 0$)

$$WSVI = r_{i2} \delta_2 \Delta S_i^* / \Delta t, \qquad WSVS = r_{s2} \delta_2 \Delta S_i^* / \Delta t,$$

$$WCON = \begin{cases} 0, & \text{if } WSVI + WSVS \geqslant r_{1wi} \Delta S_w^* / \Delta t \\ r_1 / r_{1wi} \{r_{1wi} \Delta S_w^* - \delta_2 (r_{i2} + r_{s2}) \Delta S_i^*\} / \Delta t, & \text{if } WSVI + WSVS < r_{1wi} \Delta S_w^* / \Delta t \end{cases}$$

here $r_{1wi} = (1 + L_s / C_p \cdot 5418.12 \cdot q_{sw}^* / T^{*2})^{-1}$ is the equivalent deposition coefficient, which means that because of deposition the liquid-saturation point is reached.

c2) Unsaturation with respect to liquid, but supersaturation with respect to ice ($\Delta S_w^* \leqslant 0$, $\Delta S_i^* > 0$)

$$WSVI = r_{i2}\delta_2 \Delta S_i^* / \Delta t, \quad WSVS = r_{s2}\delta_2 \Delta S_i^* / \Delta t,$$
$$WCON = \max\{r_1 \Delta S_w^* / \Delta t, \ -q_c^* / \Delta t\}.$$

c3) Unsaturation with respect to ice ($\Delta S_i^* \leqslant 0$)

$$\sum r = r_1 + \delta_2(r_{i2} + r_{s2}), \quad \text{if } r_2 \geqslant \sum r, \quad \delta_3 = 1, \quad \text{or else } \delta_3 = r_2 / \sum r,$$
$$WCON' = \max\{r_1 \delta_3 \Delta S_i^* / \Delta t, \ -q_c^* / \Delta t\},$$
$$WSVI = \max\{r_{i2}\delta_2\delta_3 \Delta S_i^* / \Delta t, \ -q_i^* / \Delta t\},$$
$$WSVS = \max\{r_{s2}\delta_2\delta_3 \Delta S_2^* / \Delta t, \ -q_s^* / \Delta t\}.$$

Recompute T^*, q_v^*, q_{sw}^*, q_c^*, ΔS_w^* and r_1. If $q_c^* > r_1\delta_3\Delta S_i^*$ and $\Delta S_w^* < 0$, $WCON = \max\{WCON' + r_1 \Delta S_w^* / \Delta t, \ -q_c^* / \Delta t\}$, or else $WCON = WCON'$.

Concentrations do not change when water is condensing or depositing. Changes occur only when it is evaporating:

$$NSVR = WSVR \cdot N_r^* / q_r^*, \quad NSVI = WSVI \cdot N_i^* / q_i^*, \quad NSVS = WSVS \cdot N_s^* / q_s^*,$$

when $WSVR < 0$, $WSVI < 0$, $WSVS < 0$ respectively.

5. *Advective Scheme for Descent of Particles*

Because the falling speed of precipitation particles is very high (in especial, raindrops), when time step is large enough, the computational scheme in flux form ($-\partial \rho g V_t \alpha / \partial \sigma$) does not meet the stability condition $V_t \Delta t / \min(\Delta\sigma) < -\rho g / P^*$. Here for descent of particles we designed an advective scheme by following the Lagrangian method. As shown in Fig.1, it is assumed that the characteristics of precipitation particles are the same in any segment of $\Delta\sigma$; $q_{\alpha m}$, $N_{\alpha m}$, V_{tm}, ρ_m represent the characteristics of precipitation particles and atmospheric density in $\Delta\sigma_m$, but at boundary surfaces σ_m, σ_{m+1}, these characteristics are discontinuous; the mass and the number of particles during falling period are assumed constant. The particles in the air column above unit area ($\Delta\sigma_m$) descend a distance of $\sigma_t = V_{tm}\rho_m g \Delta t / P^*$ with same V_{tm} and ρ_m, moves to σ', σ'', and their relative positions do not change, so that $\sigma'' = \sigma_0 + 0.5\Delta\sigma_m$, $\sigma' = \sigma_0 - 0.5\Delta\sigma_m$, $\sigma_0 = \sigma_{m+1/2} + \sigma_t$. Define $\Delta\sigma_m^k$ as the distribution of $\Delta\sigma' = \sigma'' - \sigma'$ in $\Delta\sigma_k$:

$$\Delta\sigma_m^k = \begin{cases} \Delta\sigma', & \sigma'' < \sigma_{k+1}, \ \sigma' > \sigma_k \\ \Delta\sigma_k, & \sigma'' > \sigma_{k+1}, \ \sigma' < \sigma_k \\ 0, & \sigma' > \sigma_{k+1}, \text{ or } \sigma'' < \sigma_k \\ \sigma'' - \sigma_k, & \sigma_{k+1} \geqslant \sigma'' > \sigma_k, \ \sigma' < \sigma_k \\ \sigma_{k+1} - \sigma'. & \sigma'' > \sigma_{k+1}, \ \sigma_{k+1} \geqslant \sigma' \geqslant \sigma_k \end{cases}$$

$\sum_{k=1}^{KL} \Delta\sigma_m^k = \Delta\sigma' = \Delta\sigma_m$, KL is the total number of σ levels.

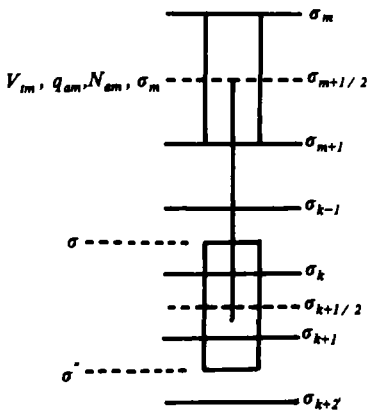

Fig. 1. Advective scheme for fall of particles (see text).

Fig. 2. Domain for case modeling. Lines a and b represent the positions of the cross sections shown in Fig.5 and Fig.9.

The change rate of α (specific mass or specific concentration) at point K due to falling is

$$\frac{\partial \alpha_k}{\partial t} = \frac{\sum_{m=1}^{KL} a_m \alpha_m - \alpha_k}{\Delta t}, \quad a_m = \frac{\Delta \sigma_m^k}{\Delta \sigma_k}, \quad m = 1,2,\cdots,KL.$$

It can be demonstrated that this scheme is unvaried and stable. This scheme is used for the descent of ice, snow and rain particles.

6. *Boundary Conditions*

Lateral boundary conditions: the time-dependent boundary condition is used for variables u, v, T and q_v; the extrapolation condition is used for momenta (P_u^*, P_v^*); the inflow / outflow-dependent condition is used for hydrometeors.

At the top and bottom of the model, $\dot{\sigma} = 0$.

III. CASE MODELING

The mesoscale vortex is one of the weather systems that lead to summer rainstorms and winter snowstorms in China. Here we simulate a summer rainstorm and a mixed winter precipitation case. In two cases at low level there are significant mesoscale cyclonic circulations. In this section we test the model's capability of modeling the circulation structure and the precipitation of meso-vortex cloud system, and compare results of several schemes with observation. The horizontal range of this model is 3000 × 3000 km, the domain is centered at (38°N, 115°E) (see Fig.2), the horizontal resolution is 90 km, the time step is 383 seconds, the top of model is on 150 hPa and there are 10 levels in vertical direction. We compare 4 models: 1) model presented here (TR model); 2) two-parameter explicit microphysical model which includes vapor and liquid water (TW model); 3) cumulus parameterization method of Kuo and Anthes (C model); 4)

dry model without water physical processes (D model). The dynamic equations and the computer schemes of these models are the same.

1. *Results of Summer Case*

From 1200 GMT 26 to 1200 GMT 27 June 1986, a severe rainstorm occurred in North China. The rainfall at surface precipitation center was 157 mm (Beijing). At 1200 GMT 26 June, the synoptic situation in Eurasian continent was the two–ridge and one–trough pattern. On 500 hPa map, the center of depression lay at (47°N, 102°E), and in East Asia there was a strong ridge, whose axis lay along 122°E. On 850 hPa map, the center of the northwest vortex lay at (37°N, 108°E). The rainstorm was a mixed cloud system and in large–scale stratiform cloud system there were activated thunderstorms. For this case Wu (1989) made the synoptic and dynamic analysis, Pan and Wang (1990) made the modeling analysis with MM4 model.

(1) *Simulations of circulation structure of vortex*

At 0000 GMT 27 June (after integration of 12 hours), on 850 hPa above the surface heavy rainfall area there was a cyclonic circulation, which corresponded well with the observed closed low pressure, and in front of vortex there was a southwest jet. On the modeled circulation field (Fig.3), the positive vorticity center was coupled with a negative vorticity center in the inflow area of the rainstorm, and the positive center, and the modeled and observed low pressure centers were nearly coincided, but the geometric center of modeled low pressure deviated from the observed one about 140 km too far north. The intensity of the modeled jet and low pressure is coincident with observation (Table 1). On 500 hPa weather map, there was a 0℃ closed warm

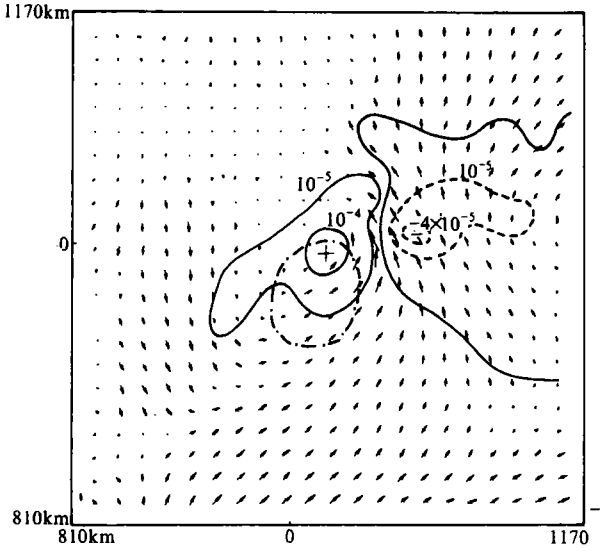

Fig. 3. The modeled wind and vorticity field of the summer case at 0000 GMT, June 27 (12–h modeling). The unit of vorticity is s^{-1}. The dot–dashed line and the sign "■" represent the observed depression and its center.

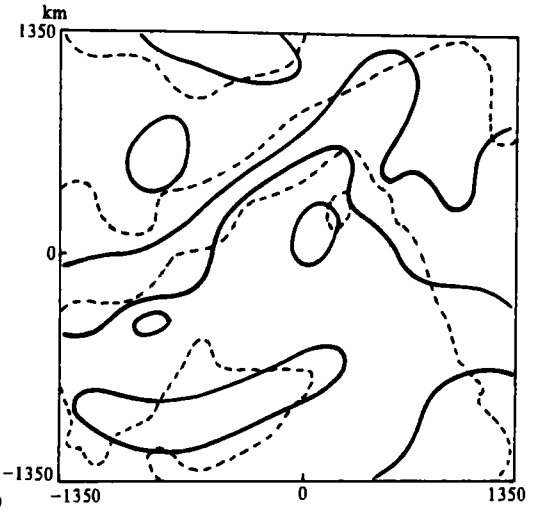

Fig. 4. Comparison between temperature field of TR model (dashed line) and observed temperature field (solid line) on 500 hPa level at 0000 GMT, June 27 (12–h modeling).

center above the vortex; correspondingly, there was a −1℃ closed warm center on the modeled field, and 3 hours later, the temperature of the modeled warm center approached 0℃ (Fig.4). From the vertical cross section through surface rainfall center it could be seen that there were two indirect circulations in front and rear of the modeled cloud system, and a direct circulation was formed between downdraft and updraft near the rear boundary of the cloud system (Fig.5). Table 1 shows the comparison results of the 4 models, it can be easily seen that all moist models (TR, TW, C), except D model, simulated well the structure of vortex. It indicates the close relation between moist physical processes and the existence and maintenance of vortex. The explicit model (TR, TW) successfully simulated the low pressure and low-level jet, but C model could not simulate the jet, whose modeled intensity of the low pressure is weaker; therefore it is clear that the results of the explicit model is more similar to observation, which is coincident with Zhang's (1989) results. For the closed warm center on 500 hPa, only the result of TR model is close to observation.

(2) *Simulation of cloud*

The simulated cloud field of TR model is consistent with the diagnostic updraft field. At the early stage of development, the body of cloud system inclines with height in agreement with the inclination of updraft, but at the mature stage, both assume vertical appearances. The modeled cloud system consists of cirrus with a content of 10^{-3}—10^{-4} g / m^3 in outflow area at upper level, deep-extended stratiform cloud over the surface precipitation area, and low level stratiform cloud in the rear, which is similar to the surface observation of cloud form (Fig.5). No cirrus

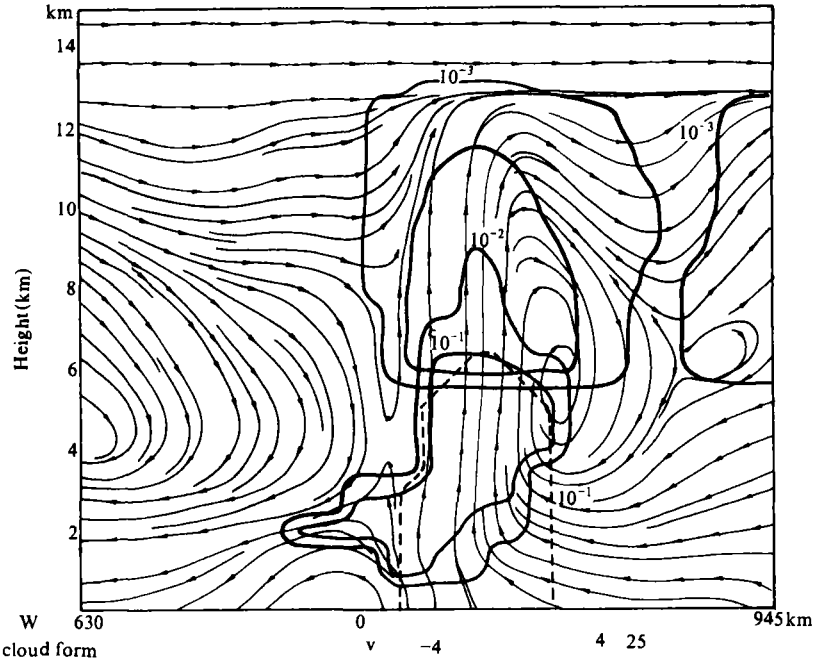

Fig. 5. Modeled cloud (upper and lower solid lines for snow and cloud respectively), rain (dashed line), and streamline field of TR model in 15-h modeling. The unit of content is g / m. The observational records of cloud form come from Zhangjiakou, Beijing, Tianjin, Dalian, Shenyang, Pyongyang (from west to east).

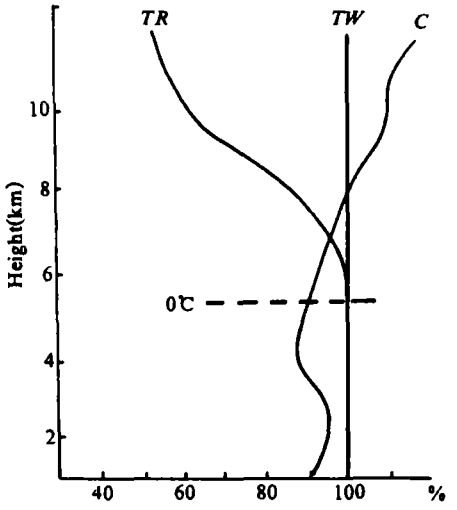

Fig. 6. Modeled relative humidity profiles of TR, TW and C models over the surface precipitation center, at 0300 GMT, June 27 (15-h modeling)

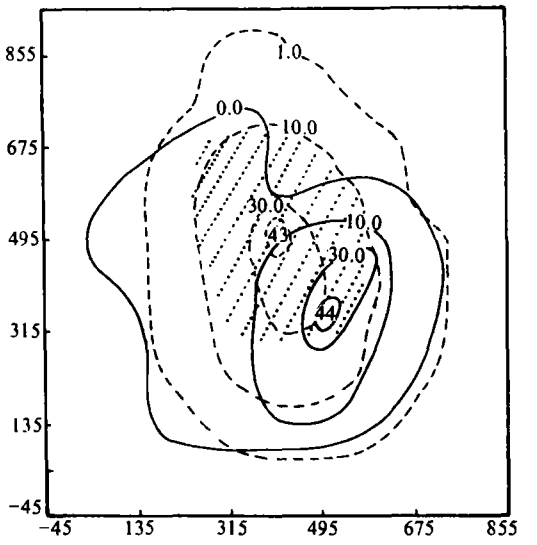

Fig. 7. Comparison between observed precipitation (solid line) and modeled precipitation of TR model (dashed line) in 18— 24 hours modeling. The shadow area and sign "▲"represent 10 mm modeled precipitation area and center of TW model.

appears on the modeled cloud field of TW model. Figure 6 is the comparison of modeled relative humidities (*RH*) in cloud system. It is obvious that the distribution of TR model is reasonable, but that of TW model is 100% from bottom to top of cloud, and that of C model, which is influenced by the given profiles of heating and moistening, is close to 110% at top but not saturated at bottom of cloud system.

(3) *Simulation of precipitation*

Radar detection shows the shape of precipitation system, like a mesoscale conglomeration, has the characteristics of low level vortex precipitation. Figure 7 is the comparison between modeled and observed precipitation. The results of TR model are close to observation, and are better than these of the other models in simulation of precipitation structure, area and rainfall center. The explicit models (TR, TW) are worse than C model in the first 6-h rainfall modeling, but their capability of persistence forecasting is much better than that of C model (Table 2). In the first 6 hours (from 2000 GMT 26 to 0200 GMT 27 June) there was a small rainfall center to the south of the main precipitation area according to observation, and none of the models above simulated it successfully.

2. *Results of Winter Case*

From 1200 GMT 27 to 0000 GMT 28 January 1990, a mesoscale mixed precipitation process occurred in North and East China, especially heavy snow in the north part of Shandong Province, Henan Province and North China. The maximum snowfall was 16 mm at Jinan. On 700 hPa map at 1200 GMT 27 January, a pressure ridge lay along the Ural Mountains, a

pressure trough lay to the east of Bajkal Lake and moved southeastward fast. From Sichuan Basin to Hetao area lay a trough, before which there was a large area of warm and moist air flow from southwest to northeast with a maximum wind speed of 20 m / s. Yang (1990) analysed this case in detail.

(1) *Simulation of circulation and vortex structure*

On the initial field there was no cyclonic circulation at low level and surface, but along with the development of precipitation, a cyclonic circulation on surface was formed gradually. TR model produced a closed positive vorticity center with a central value of 9.8×10^{-5} / s on 700 hPa in the area with the sharpest cyclonic curvature. The closed positive vorticity center was coupled with a closed negative vorticity center (central value -4.5×10^{-5} / s), and then the vorticity couple kept stable and moved to east. At 0000 GMT 28 January, the closed positive vorticity areas on 700 hPa and 850 hPa were right over the surface cyclonic circulation, the center of which was in agreement with the observation very well (Fig.8). Compared with TR model, TW model also produced the surface cyclonic circulation, but the vorticity intensity was weaker. C and D models did not produce the surface circulation (Table 1).

(2) *Simulation of cloud*

For TR model, the modeled phase distribution of cloud and precipitation and the extended

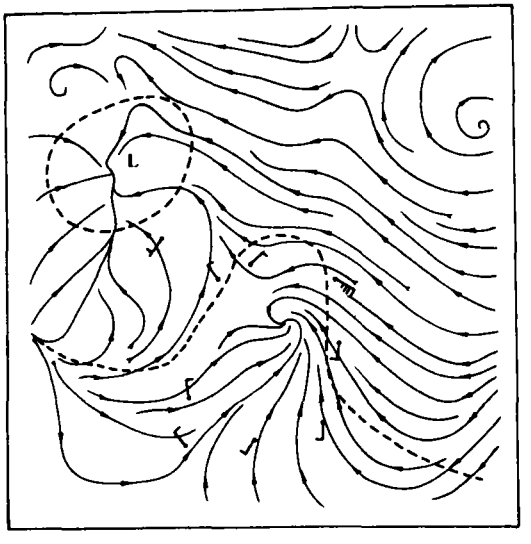

Fig. 8. Modeled surface streamline field, compared with observed wind and sea level pressure field (dashed line).

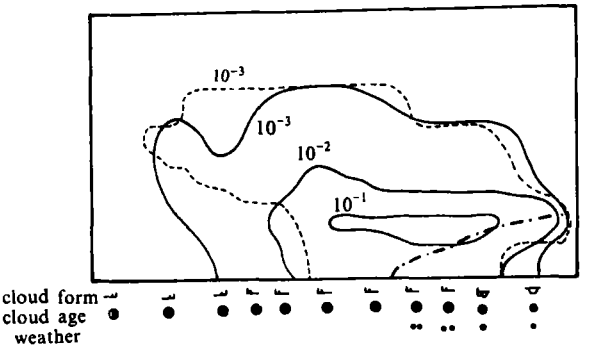

Fig. 9. Modeled cloud system field of TR model (solid line) and TW model (dashed line) at 0000 GMT 28 January. The records of cloudage, cloudform and weather come from the following stations (from north to south): Hailar, Arxan, Lindong, Chifeng, Jinzhou, Tianjin, Jinan, Qingdao, Bengbu, Nanjing, Anqing. The dot-dished line represents 0℃ isothermohyps.

range of cloud body are close to observations (Fig.9), but for TW model, the modeled rain area is obviously smaller than that of observation, and the phase distribution can not be described. From Fig.9 we can find out the close relation between the modeled water content distribution of TR model and the surface observational records of cloudage.

(3) *Simulation of precipitation*

The observed distribution of 6–h accumulated precipitation is not homogeneous. The snowfall of precipitation center is 2 or 3 times as much as that of the surrounding area. But in a large area the precipitation is nearly homogeneous; the snowfall in most areas is 2 to 7 mm. For TR model, the amount and range of modeled precipitation and the modeled boundary between rain and snow are similar to observations. TR model also produced a belt of mixed precipitation (Fig.10). For TW model the modeled precipitation amount and range are smaller than these of observations obviously, especially in snow region. It indicates that to simulate cloud and precipitation in winter we must consider microphysical processes in all water phases. The modeled precipitation amount of C model in first 6 hours is better than that of the other models, but the persistent modeling capability of C model is poorer (Table 2).

IV. SUMMARY

The case studies demonstrate that for description of the circulation structure and the development of precipitation of a cloud system, the model with more detailed microphysical processes (explicit model) is better than the model with simple cloud physical processes (as C model

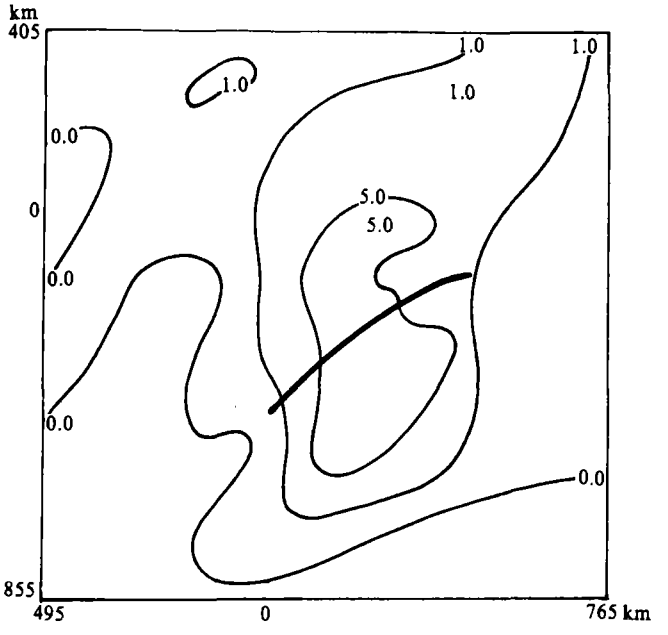

Fig. 10. The observed (solid line) and modeled (dashed line for TR model) precipitation fields in 6—12 hours, and the shadow area represents 1 mm precipitation area of TW model. The double–dashed line represents the modeled boundary belt between rain and snow of TR model.

Table 1. Comparison between Observed and Modeled Structures

Structure of vortex	Center of depression (grid)	Intensity of depression (10 m)	Wind speed of jet (m / s)	Center of vortex (grid)	Intensity of vortex (10 / s)	Closed warm center on 500 hPa	Center of vortex (grid)	Intensity of vortex (10 / s)	Center of circulation (grid)
Observed	17, 17.5	135.0	18	—	—	0℃	—	—	11, 18
TR	18, 18	135.6	18	18, 17	14.1	−1℃	11, 18	6.4	11, 18
TW	18, 18	135.6	18	18, 17	13.6	—	11, 18	6.1	11, 18
C	15, 17	137.2	9	16, 18	3.9	—	11, 17	5.9	—
D	—	—	5	—	—	—	—	—	—

Note: The data of depression, wind, vorticity are from 850 hPa level, in 12-h modeling. The vorticity of observational field is not calculated.

Table 2. Comparison between Observed and Modeled Precipitation

Case	Summer case				Winter case			
Precipitation	Rain				Rain	Snow	Rain	Snow
Period	0—6 h	6—12 h	12—18 h	18—24 h	0—6 h		6—12 h	
Observed	48	129	132	44	12	11	16	7
TR	11 (45)	34 (97)	59 (154)	43 (201)	3.8 (20)	5.5 (165)	5.1 (50)	7.3 (178)
TW	11 (100)	33 (186)	76 (270)	43 (284)	—	4.4 (251)	—	4.5 (150)
D	33 (135)	21 (97)	22 (207)	16 (371)	—	7.1 (191)	—	4.8 (273)

Note: The unit of precipitation is mm. The figures in parentheses are the differences of observed and modeled precipitation centers, in km.

presented here), and the model without microphysical processes (D model) can not describe the characteristics of the cloud system' s circulation. The model presented here is better than the others in description of cloud field, distribution of related humidity, dynamic structure and surface precipitation of cloud systems in these two cases, which indicates that the physical processes in the mixed-phase cloud system model is closer to these in the real atmosphere than in the other models. Since we selected a set of proper hybrid computer schemes and disposed of the microphysical processes with special method, the computational stability, conservation and accuracy of the model in a large time step are ensured, so that it could be used not only in modeling studies of the mesoscale precipitation processes and dynamic processes in the atmosphere, but also as a supplementary tool for the forecasting of mesoscale weather systems.

REFERENCES

Anthes, R. A. and Warner, T. T. (1978), Development of hydrodynamic models suitable for air pollution and other

mesometeorological studies, *Mon. Wea. Rev.*, **106:** 1045—1078.

Anthes, R. A., E.-Y. Hsie and Y.-H. Kuo (1987), Description of the Penn State / NCAR Mesoscale Model Version 4 (MM4), *NCAR Tech. Note*, NCAR / TN-282.

Brown, J. and Campana, K. (1978), An economical time-differencing system for numerical weather prediction, *Mon. Wea. Rev.*, **106:** 1125—1136.

Buekov, M. V. and Pernach, A. M. (1975), Numerical simulation of microphysical processes of precipitation formation in mixed stratiform clouds, Ezv. A N. USSR, *Physics of Atmosphere and Ocean*, **11:** 469 (in Russian).

Heimann, D. (1990), Three-dimensional modeling of synthetic cold fronts approaching the Alps, *Meteor. Atmos. Phys.*, **42:** 197—219.

Hu Zhijin and He Guanfang (1987), Numerical simulation of microprocesses in cumulonimbus clouds (I)——Microphysical model, *Acta Meteor. Sin.*, **45:** 467—484 (in Chinese).

Hu Zhijin and Yan Caifan (1986), Numerical simulation of microphysical processes in stratiform clouds (I)——Microphysical model, *Journal of Academy of Meteorological Sciences*, SMA, China, **1:** 37—52 (in Chinese).

Liu Yubao, Hu Zhijin and You Laiguang (1988), A study of the frontal snowfall in Junggar Basin of Xinjiang in winter——Part II: Theoritical discussion, *Journal of Academy of Meteorological Sciences*, SMA, China, **3:** 159—168 (in Chinese).

Mason, B. J. (1971), *The Physics of Clouds*, Appendix B.3.2, 2nd ed., Oxford University Press, London, 608pp.

Pan Zaitao and Wang Pengyun (1990), Numerical simulation of the 26— 27 June 1986 heavy rainfall in Beijing-Tianjin-Hebei area, *Quarterly Journal of Applied Meteorology*, **1:** 242—252 (in Chinese).

Pernach, A. M. (1988), Mathematical modeling of evolution of warm frontal cloud system (three-dimensional model), *Trude Uxr. NEE.*, **229:** 121—142 (in Russian).

Rutledge, S. A. and Hobbs, P. V. (1983), The mesoscale and microscale structure and orgnization of clouds and precipitation in midlatitude cyclones——VIII: A model for the "seeder-feeder" process in warm frontal rainbands, *J. Atmos. Sci.*, **40:** 1186.

Soony, Su-Tzai and Ogura, Y. (1973), A comparison between axisymmetric and slabsymmetric cumulus cloud models, *J. Atmos. Sci.*, **30:** 879.

Wu Zhenghua (1989), An analysis of severe rainstorm by two meso-vortices, *Journal of Academy of Meteorological Sciences*, SMA, China, **4:** 291—299 (in Chinese).

Yang Xiuzhen (1990), Monthly weather, *Meteorological Monthly*, **16(4):** 58—61 (in Chinese).

You Laiguang et al. (1982), Observation and analysis of ice nuclear concentration in troposphere, *Collected Papers of Meteorological Science and Technology*, **2:** 141—144 (in Chinese).

Zhang Dalin (1989), The effect of parameterized ice microphysics on the simulation of vortex circulation with a mesoscale hydrostatic model, *Tellus*, **41(A):** 132—147.